Electronic Supplementary Material (ESI) for Journal of Materials Chemistry C.

Efficient Microwave Traps with Markedly Enhanced Interfacial Polarization and Impedance Matching Enabled by Dual-Shelled, Dual-Cavity Magnetic@Dielectric Hollow Nanospheres

Jiasong Hua, Wenjun Ma, Xiaoyun Liu, Qixin Zhuang, Zeyang Wu, Huang Huang, and Shaoliang Lin**

J. Hua, W. Ma, Prof. X. Liu, Prof. Q. Zhuang, Z Wu, H. Huang, Prof. S. Lin
The Key Laboratory of Advanced Polymer Materials of Shanghai, School of Materials Science and Engineering, East China University of Science and Technology, Shanghai 200237, China
E-mail: qxzhuang@ecust.edu.cn (Q.Z.) and slin@ecust.edu.cn (S.L.)

Figures and Figure Captions

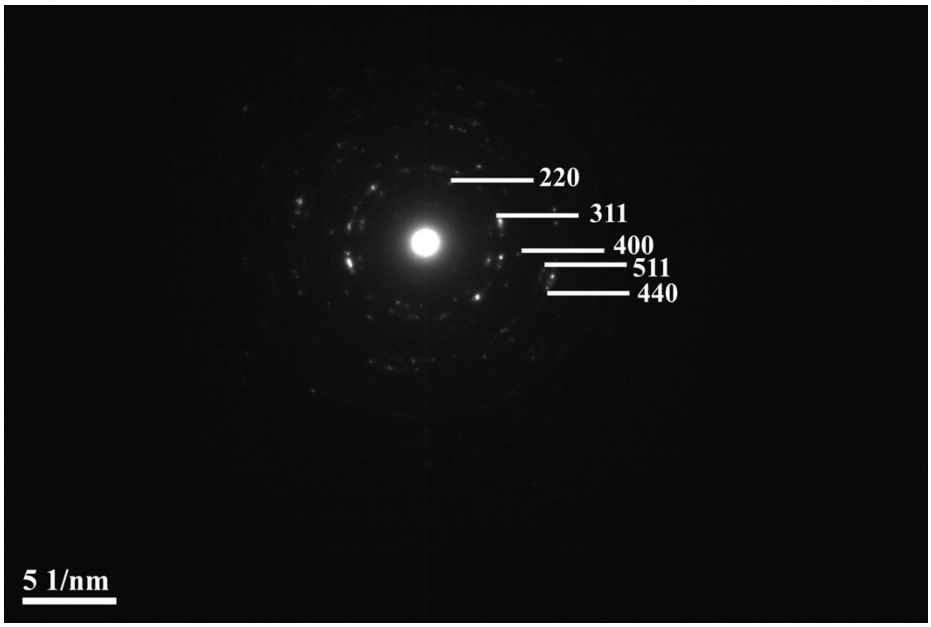

Figure S1. Selected-area electron diffraction (SAED) pattern of Fe_3O_4 hollow spheres (i.e., Fe_3O_4-HNs).

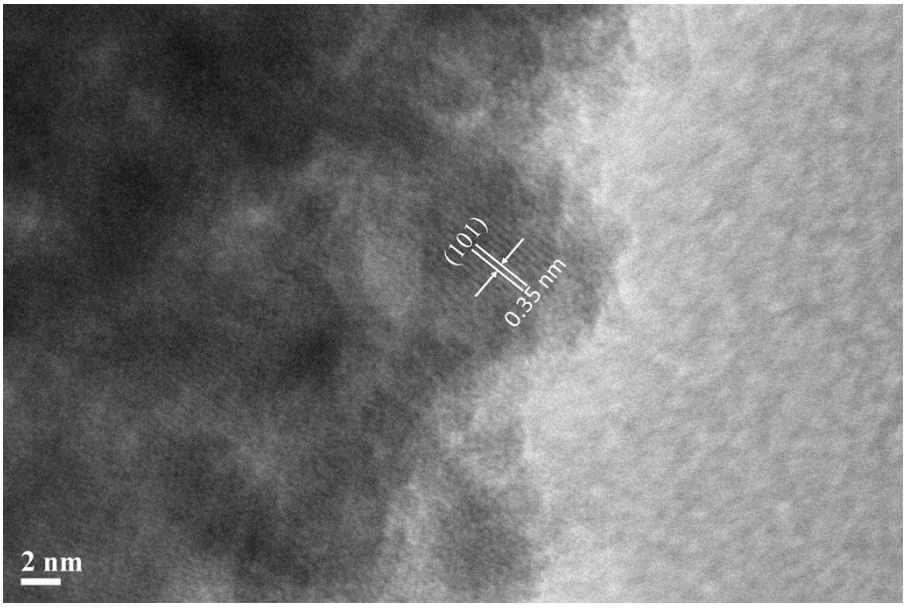

Figure S2. HRTEM image of the outer TiO_2 shell on a single dual-shelled Fe_3O_4@TiO_2 hollow nanosphere (i.e., DS-Fe_3O_4@TiO_2-HN).

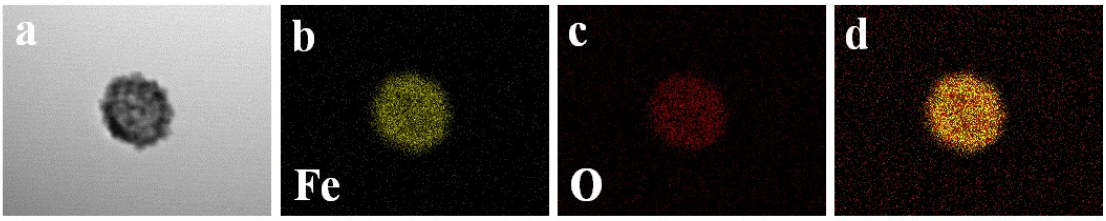

Figure S3. (a) TEM and (b-d) energy-dispersive X-ray spectroscopy (EDX) elemental mappings of a single Fe_3O_4 hollow sphere (i.e., Fe_3O_4-HN): (b) Fe, (c) O, and (d) combined.

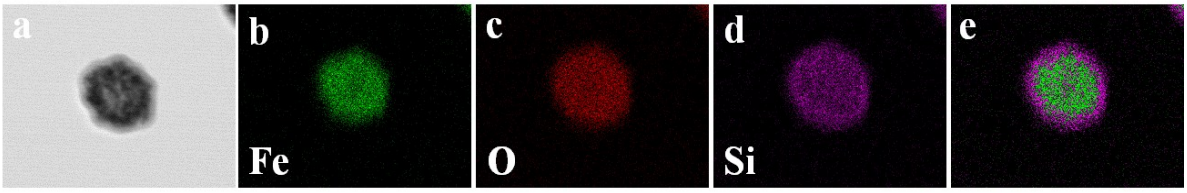

Figure S4. (a) TEM and (b) EDX elemental mapping of a single Fe_3O_4@SiO_2 hollow nanosphere (i.e., Fe_3O_4@SiO_2-HN): (b) Fe, (c) O, (d) Si, and (e) combined.

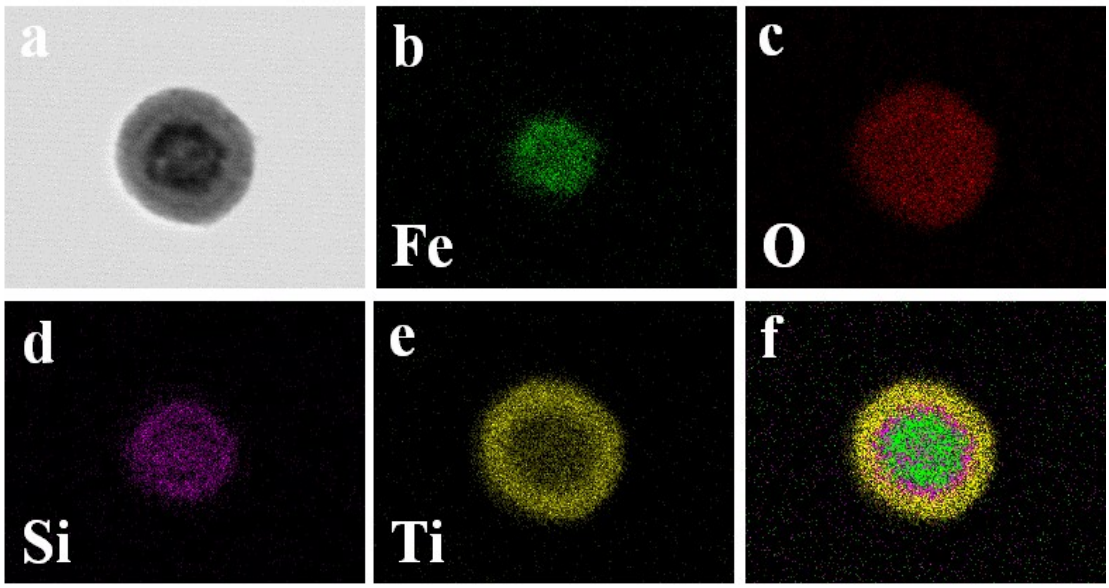

Figure S5. (a) TEM and (b) EDX elemental mapping of a single Fe_3O_4@SiO_2@TiO_2 hollow nanosphere (i.e., Fe_3O_4@SiO_2@TiO_2-HN): (b) Fe, (c) O, (d) Si, (e) Ti, and (f) combined.

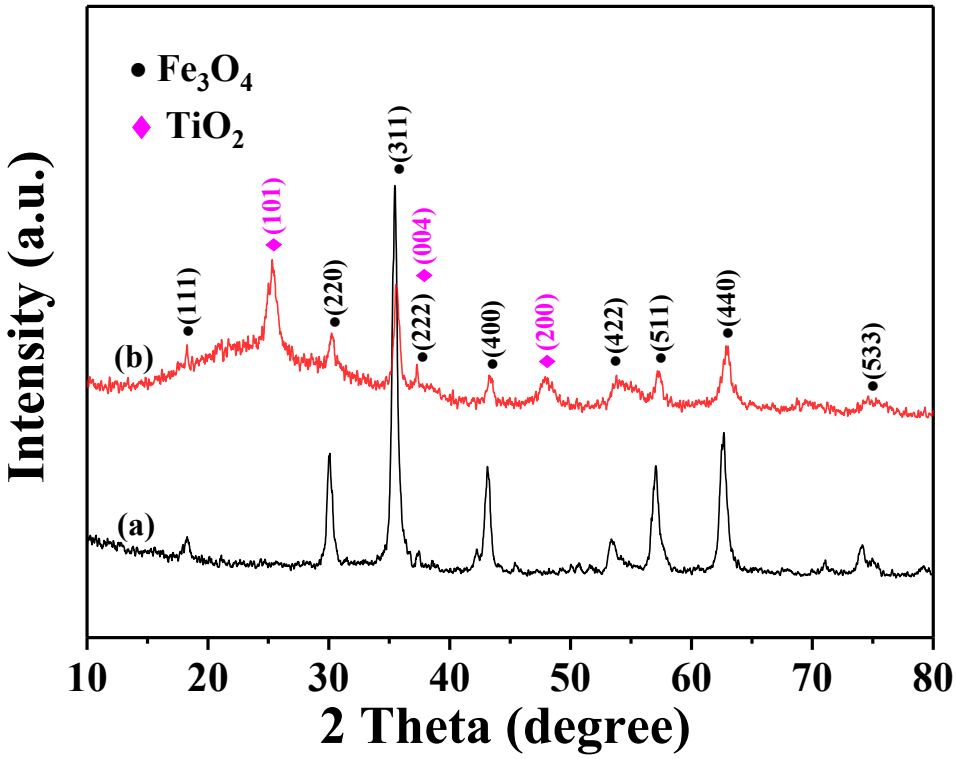

Figure S6. XRD patterns of (a) Fe_3O_4 hollow spheres (i.e., Fe_3O_4-HNs) and (b) dual-shelled Fe_3O_4@TiO_2 hollow nanospheres (i.e., DS-Fe_3O_4@TiO_2-HNs).

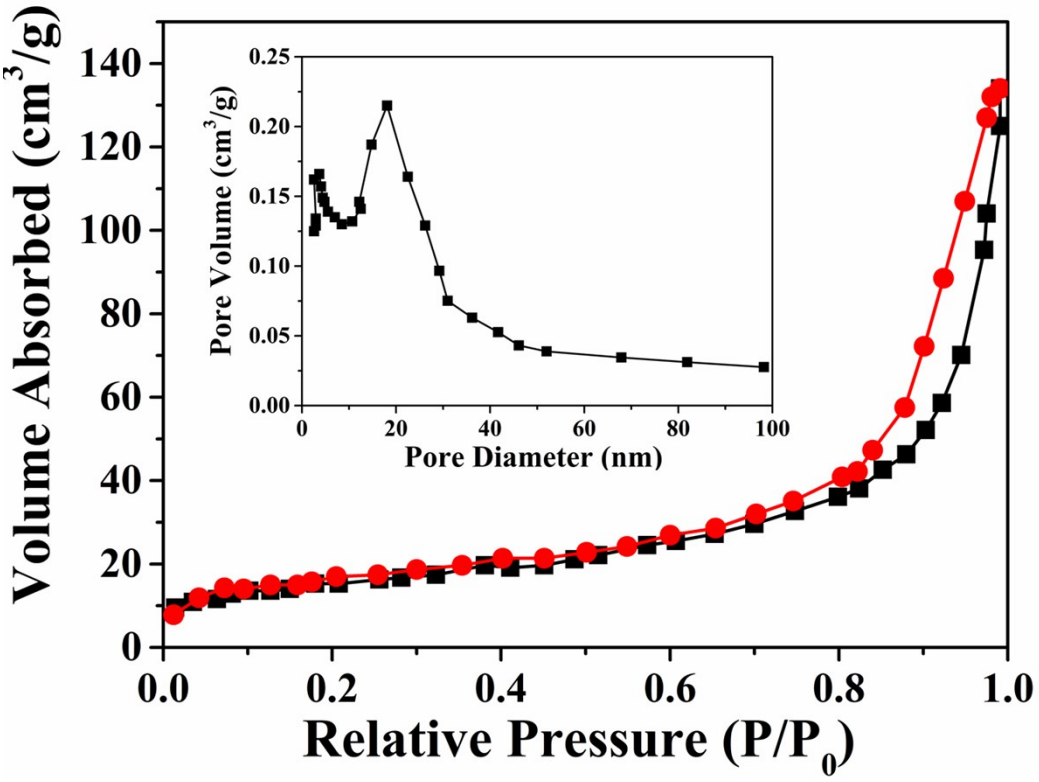

Figure S7. Nitrogen sorption isotherms and corresponding pore size distribution curve (inset) of DS-Fe_3O_4@TiO_2-HNs.

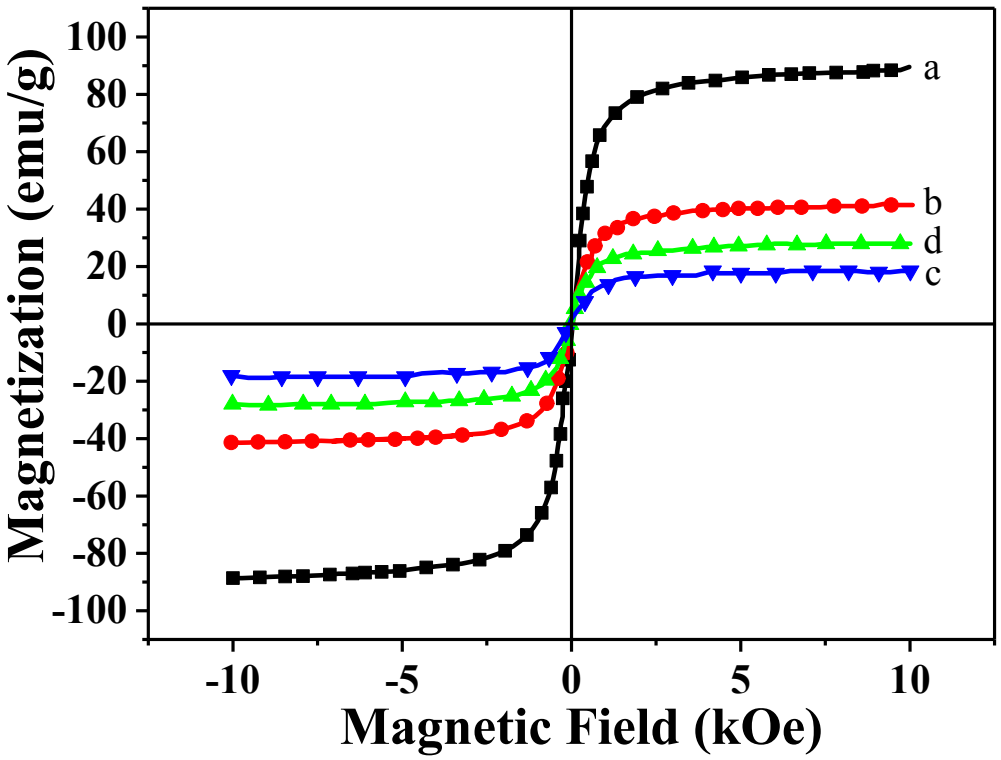

Figure S8. Hysteresis loops of (a) Fe_3O_4-HNs, (b) Fe_3O_4@SiO_2-HNs, (c) Fe_3O_4@SiO_2@TiO_2-HNs, and (d) DS-Fe_3O_4@TiO_2-HNs.

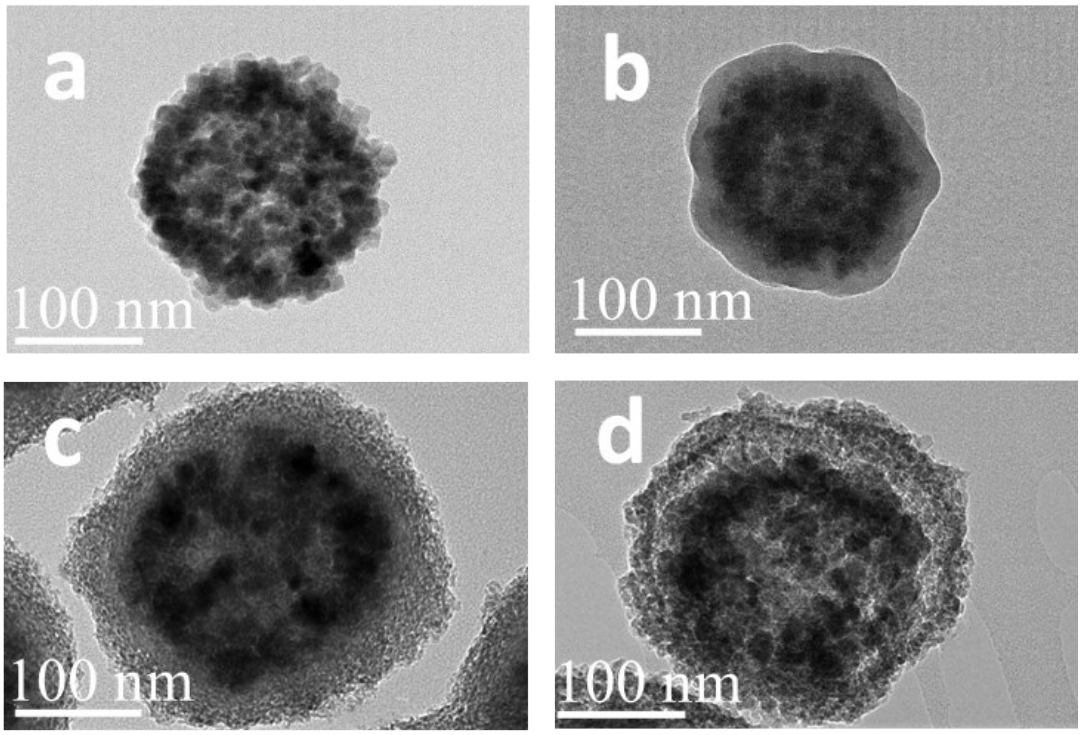

Figure S9. TEM images of (a) Fe_3O_4-HNs, (b) Fe_3O_4@SiO_2-HNs-40-20, (c) Fe_3O_4@SiO_2@TiO_2-HNs-40-20-20, and (d) DS-Fe_3O_4@TiO_2-HNs-40-20-20.

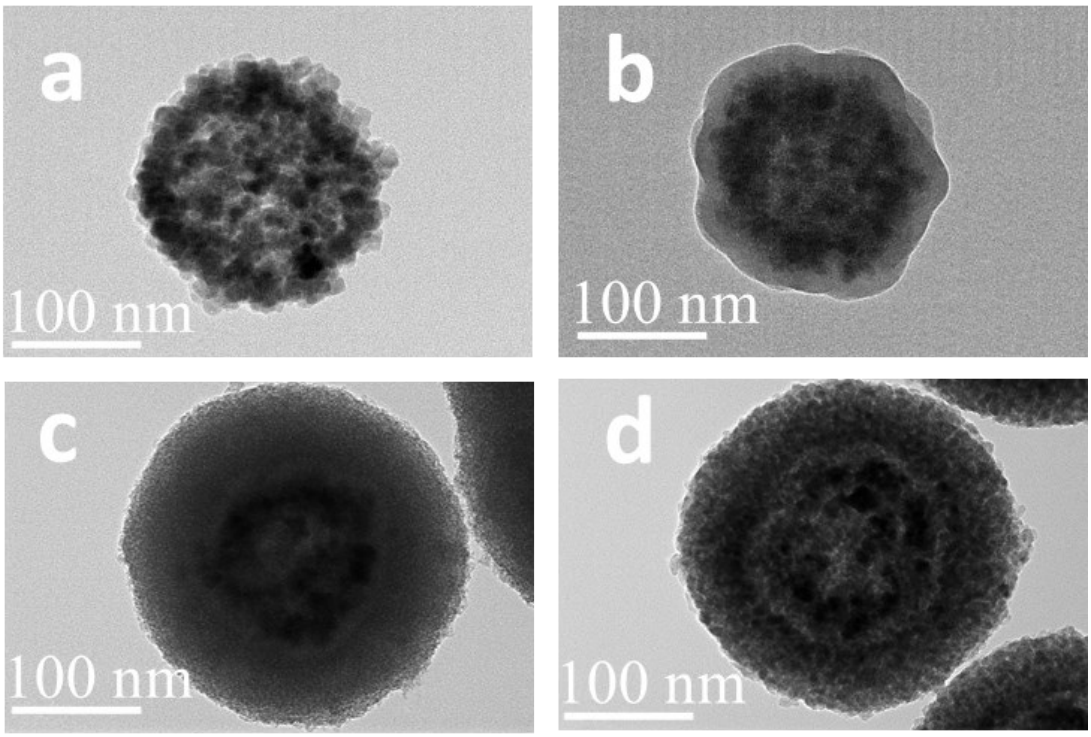

Figure S10. TEM images of (a) Fe_3O_4-HNs, (b) Fe_3O_4@SiO_2-HNs-40-20, (c) Fe_3O_4@SiO_2@TiO_2-HNs-40-20-60, and (d) DS-Fe_3O_4@TiO_2-HNs-40-20-60.

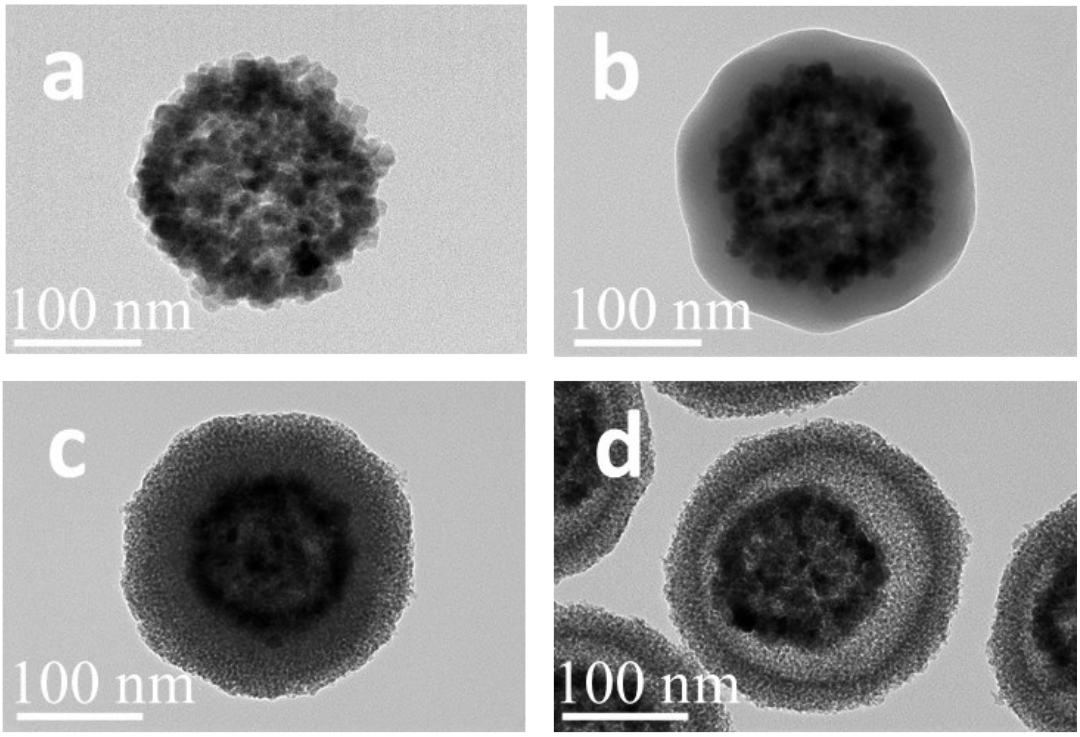

Figure S11. TEM images of (a) Fe_3O_4-HNs, (b) Fe_3O_4@SiO_2-HNs-40-40, (c) Fe_3O_4@SiO_2@TiO_2-HNs-40-40-40, and (d) DS-Fe_3O_4@TiO_2-HNs-40-40-40.

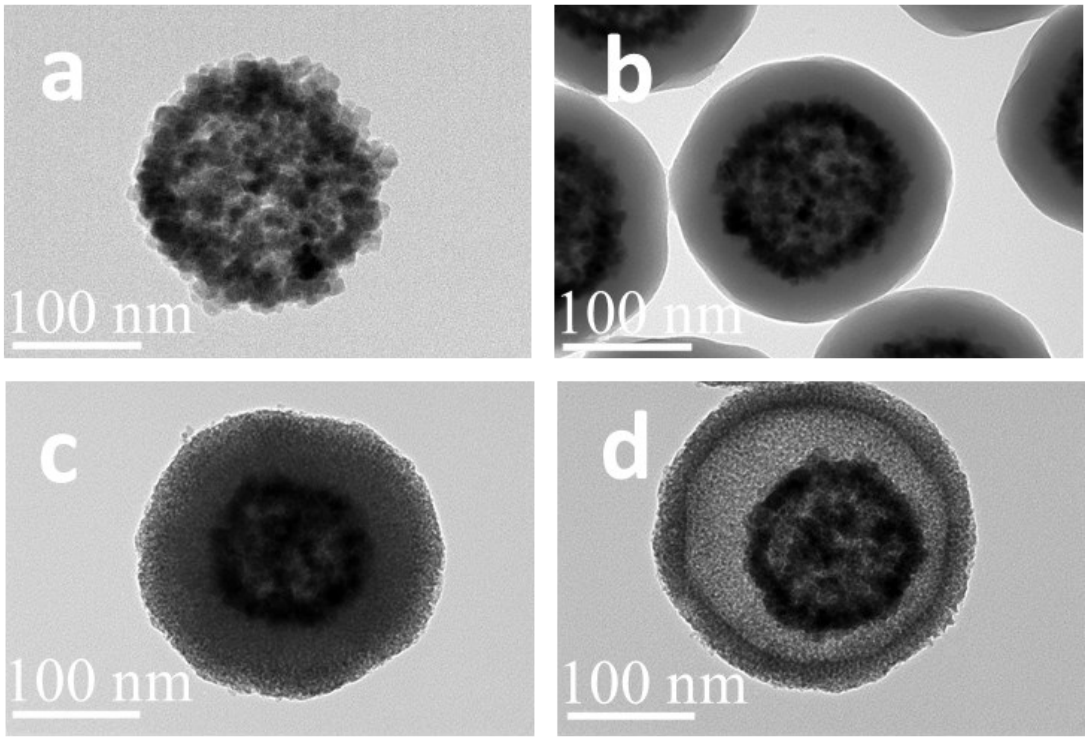

Figure S12. TEM images of (a) Fe_3O_4-HNs, (b) Fe_3O_4@SiO_2-HNs-40-60, (c) Fe_3O_4@SiO_2@TiO_2-HNs-40-60-40, and (d) DS-Fe_3O_4@TiO_2-HNs-40-60-40.

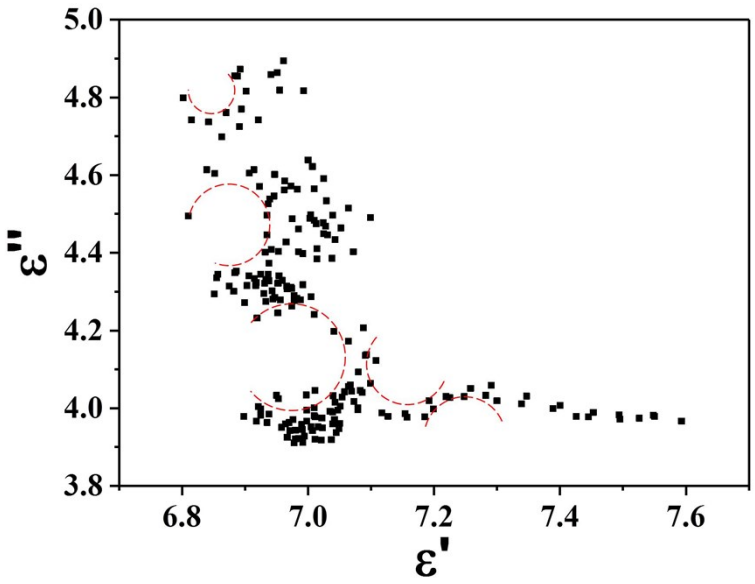

Figure S13. Dielectric Cole-Cole semicircles of DS-Fe_3O_4@TiO_2-HNs.

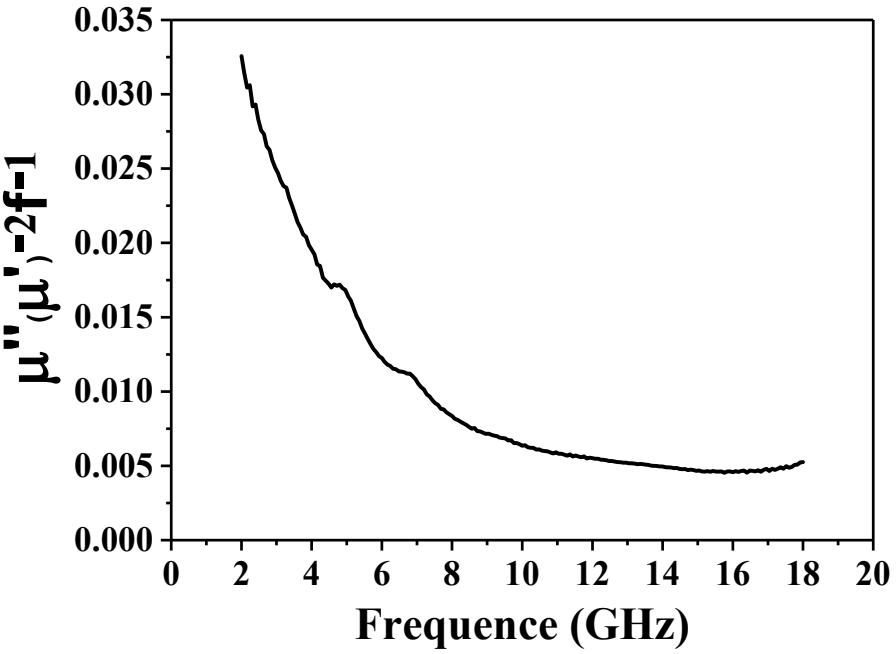

Figure S14. Frequency-dependent eddy current loss plot of DS-Fe_3O_4@TiO_2-HNs.

Table S1. Summary of microwave absorption properties of the state-of-the-art absorbers

Types of absorber	**Thickness (mm)**	**Reflection loss minimum, RL_{min} (dB)**	**Effective bandwidth (< −10 dB) (GHz)**	**Frequency range (< −10 dB) (GHz)**	**Refs.**
RGO/Fe_3O_4/Fe	4	-23.09	3.9	7.4-11.3	2 (2016)
Fe_3O_4/C	2	-20.60	3.8	11.8-15.6	3 (2014)
Fe_3O_4/CuSilicate	2	-23.50	10.4	3.5-13.9	4 (2013)
CoNi/SiO_2/TiO_2	2.1	-58.20	8.1	8-16.1	1 (2016)
RGO/Fe_3O_4	2	-15.38	2.8	10.4-13.2	5 (2013)
$CoFe_2O_4$/RGO	2.8	-57.70	5.8	8.3-14.1	6 (2018)
Carbon/ Fe_3O_4	1.6	-32.00	2	10.5-12.5	7 (2015)
FeCo/C/$CoFe_2O_4$	6	−25.80	7.2	10.8-18	8 (2016)
DS-Fe_3O_4@TiO_2-HSs	**1.8**	**−60.17**	**10.5**	**7.5-18**	**This work**

References

1. Liu Q, Cao Q, Bi H, Liang C, Yuan K, She W*, et al.* $CoNi@SiO_2@TiO_2$ and $CoNi@Air@TiO_2$ Microspheres with Strong Wideband Microwave Absorption. *Adv. Mater.* **2016**, *28*, 486-490.
2. Ding Y, Zhang L, Liao Q, Zhang G, Liu S, Zhang Y. Electromagnetic Wave Absorption in Reduced Graphene Oxide Functionalized with Fe_3O_4/Fe Nanorings. *Nano Res.* **2016**, *9*, 2018-2025.
3. Du Y, Liu W, Qiang R, Wang Y, Han X, Ma J*, et al.* Shell Thickness-Dependent Microwave Absorption of Core-Shell Fe_3O_4@C Composites. *ACS Appl. Mater. Interfaces* **2014**, *6*, 12997-13006.
4. Fang J, Liu T, Chen Z, Wang Y, Wei W, Yue X*, et al.* A Wormhole-Like Porous Carbon/Magnetic Particles Composite as an Efficient Broadband Electromagnetic Wave Absorber. *Nanoscale* **2016**, *8*, 8899-8909.
5. Sun X, He J, Li G, Tang J, Wang T, Guo Y*, et al.* Laminated Magnetic Graphene with Enhanced Electromagnetic Wave Absorption Properties. *J. Mater. Chem. C* **2013**, *1*, 765-777.
6. Liu Y, Chen Z, Zhang Y, Feng R, Chen X, Xiong C*, et al.* Broadband and Lightweight Microwave Absorber Constructed by in Situ Growth of Hierarchical $CoFe_2O_4$/Reduced Graphene Oxide Porous Nanocomposites. *ACS Appl. Mater. Interfaces* **2018**, *10*, 13860-13868.
7. Wang J, Zhou H, Zhuang J, Liu Q. Magnetic [Gamma]-Fe_2O_3, Fe_3O_4, and Fe Nanoparticles Confined within Ordered Mesoporous Carbons as Efficient Microwave Absorbers. *Phys. Chem. Chem. Phys.* **2015**, *17*, 3802-3812.
8. Feng Y, Li D, Jiang L, Dai Z, Wang Y, An J*, et al.* Interface Transformation for Enhanced Microwave-Absorption Properties of Core Double-Shell Nanocomposites. *J. Alloys Compd.* **2017**, *694*, 1224-1231.